

# Numerical and experimental investigation of laser induced tube bending

Wenchuan Li and Y. Lawrence Yao  
Department of Mechanical Engineering, Columbia University  
New York, NY 10027, USA

## Abstract

Mechanisms of the process are examined to better understand the deformation characteristics such as slightly protruded shape at the intrados, wall thickness variation, cross-section ovalization, bending radius, and asymmetry. A finite element model is developed and validated by experimental observations. Factors important to characteristics of deformation are experimentally and numerically investigated. Temperature and stress/strain distributions obtained from the simulation models are also used to better understand additional phenomena accompanying the process, and to help devise ways to improve the process such as reducing asymmetry. The process effects on hardness and microstructure variations are also reported.

## 1 Introduction

Tube bending is important in the manufacturing of boilers, engines, heat exchangers, air conditioners, and tubing and pipe products. Laser bending of tubes has the following advantages over mechanical bending of tubes. Neither a hard bending tool nor external forces are required, and thus the cost of tube bending is greatly reduced for small-batch production and prototyping. Wall thickness reduction seems to be avoided and lesser ovalization results. With the flexibility of the laser beam delivery and numerical control systems, it is easier to automate the process. Tube laser bending has the potential to deal with materials whose bending normally requires repeated annealing when mechanical bending is used. Silve, et al. investigated procedures for laser bending of square cross-section tubes of mild steel<sup>1</sup>. Different scanning sequences were compared experimentally. Laser shaping of tubes and the microstructure of formed parts was investigated<sup>2</sup>, but no details were given. Kraus<sup>3</sup> conducted a FEM study of laser bending of square cross-section tubes and studied the temporal development of plastic straining and restraining in the bending process. The sequence of heating was also investigated by the simulation but no experimental validation was conducted. In the present work, the mechanism of tube laser bending is studied in more detail through numerical and experimental investigations. The causes for various aspects of deformation characteristics such as wall thickness variation, ovalization, protruded intrados, and bending radius are explained.

## 2 Mechanism of laser bending of tubes

It is generally known that laser bending of tubes is achieved through the upsetting mechanism. Consider the circular tube shown in Fig. 1. The tube rotates typically 180 degrees or more when its outer circumference is heated by a laser beam. The laser beam size is so chosen that it is much greater than the tube thickness. As a result, the scanned region of the tube is heated almost

homogeneously in the thickness direction, and undergoes compressive plastic deformation and wall thickening due to restriction on thermal expansion by the surrounding material. The shortening in the scanned region (in the axial direction of the tube) subsequently causes the tube to bend towards the laser beam.

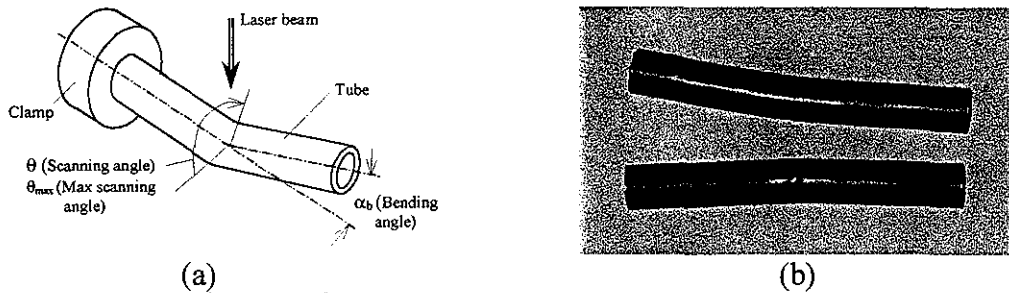


Fig. 1 (a) Schematic of laser bending of tubes (b) Samples of laser bent tubes (outer diameter 12.7 mm and thickness 0.89 mm)

A more detailed examination of the upsetting mechanism may help better understand the bending process. The thermally induced compressive stresses are exerted on the heat-affected region in both the axial and circumferential direction as shown in Fig. 2. The axial stress is more significant and is primarily responsible for the wall thickening, while the vertical component of the circumferential stress tends to make material in the area move outward. Therefore, the deformation in the region is a combination of the shortening along the axial direction of the tube and the displacement outward in the radial direction.

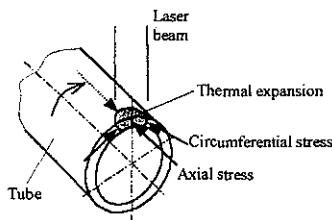


Fig. 2 Direction of thermal – induced stresses

Since laser bending of tubes is mainly made possible by the axial plastic shortening at the intrados via the above-mentioned mechanism, the tensile deformation at the extrados is much less than that in mechanical bending. By properly adjusting process parameters, the wall thinning at the extrados can be greatly reduced or nearly avoided.

For the same reason, the minimum bending radius in laser forming of tubes is not determined by the tensile failure at the extrados. This means the elongation of the material and the outer diameter may no longer be the main factors affecting the minimum bending radius as in mechanical bending. Other parameters such as laser beam diameter may play a more important role in determining the minimum bending radius.

In mechanical bending, ovalization is caused by the external force exerted by the bending die at the intrados as well as the significant tensile stress at the extrados. The ovalization in laser bending however is smaller than that in mechanical bending because no die is used and tensile stress at the extrados is greatly reduced.

### 3 Experiment

As stated earlier, it is essential that the ratio of laser beam diameter,  $d$ , to tube thickness,  $t$  is high so that there is no steep temperature gradient in the direction of the wall thickness. The chosen

ratio  $d/t$  ranges from 12.4 up to 16.9. The thickness of the tube is 0.89mm and length 100 mm. The material of the tube is low carbon steel AISI 1010. To increase coupling of laser power, the samples were coated with graphite after cleaning using propanol. During scanning, one end of the tube was clamped as shown in Fig. 1. Each tube was scanned ten times with still air cooling in-between except one case indicated in the discussion section where forced air cooling was used. The CO<sub>2</sub> laser system used has the maximum power of 1.5 kW. The power density used is Gaussian distribution (TEM<sub>00</sub>). Laser beam diameter is defined as the diameter at which the power density becomes  $1/e^2$  of the maximum power value. The process parameters used in this work are shown in Table 1, which are also used in simulation.

Table 1 The experimental and simulation conditions for laser forming of tubes

No.	Power (W)	Scanning speed (rad/s)	Beam diam. (mm)	Max scanning angle, $\theta_{max}$ (deg)	Ratio $D/t^*$
1	780	1.57-2.63	11	180	14.3
2	780, 1200	1.57, 2.63	11	180-322	14.3
3	500-780	1.57	11	180	14.3
4	780	1.57	11-15	270	14.3-28.5

\*  $D$  is the tube outer diameter and  $t$  the wall thickness

The displacement and the bending angle of the tube were measured by a coordinate measuring machine. The microstructures of the unprocessed and bent tubes were observed using a scanning electron microscope after the samples were etched using 3% HNO<sub>3</sub> for 20 seconds.

#### 4 Numerical simulation

In the model of the finite element analysis (FEA), nonlinear analysis is used because of characteristics of the laser bending process of tubes. In the creation of mesh seed, a cluster function is so used along the axial direction of the tube that there is a denser mesh area with larger width near scanning path as compared with using one way bias. That is better for the tubing forming process associated with the large beam diameter. The same mesh is created for both thermal and structural analyses. In the FEA numerical simulation using code ABAQUS, three-dimensional heat-transfer elements with eight nodes DC3D8 and continuum stress/displacement elements with the same dimension and number of nodes C3D8 are used for the thermal and structural analyses respectively<sup>4</sup>. A user-defined subroutine is developed using FORTRAN to define the magnitude of the heat flux generated by the laser beam for specific positions, which depends on the coupled laser power, beam diameter, scanning speed, and scanning scheme.

The following assumptions are made for the numerical modeling. Heat generated by plastic deformation is small compared with heat input by laser beam so that it can be neglected. A sequential thermal-mechanical analysis, therefore, is used in the simulation. Heating and deformation are symmetrical about the scanned plane and therefore only half tube is simulated. No melting occurs during the laser forming process. The tube under analysis is isotropic and work hardening material. The total deformation consists of the elastic strain, plastic strain, and thermal strain.

The boundary conditions used are as follows. No movement across the scanning plane (plane of symmetry) takes place during laser forming of the tubes. Surface free convection  $q = h(T - T^o)$ ,

where  $h = h(x, t)$  is the film coefficient, and  $T^o = T^o(x, t)$  the surrounding temperature, and radiation  $q = A((T - T^z)^4 - (T^o - T^z)^4)$ , where  $A$  is the radiation constant and  $T^z$  the absolute zero on the temperature scale used. The symmetric plane is under the adiabatic condition.

In numerical simulation, a general Hooke's law is used for elastic deformation and Von Mises criterion is used as the yield criterion. Plastic deformation of the workpiece follows the flow rule. In this simulation, the isotropic hardening rule is adopted. The relationship between the flow stress and strain is given by  $\sigma = C\varepsilon^n$ , where  $\sigma$  is the flow stress,  $\varepsilon$  the strain,  $n$  the work-hardening exponent,  $C$  is the strength coefficient. The influence of strain rate on flow stress is also taken into account<sup>5</sup>. Temperature dependent material properties, such as thermal conductivity, specific heat, Young's modulus, and flow stress are also considered in the numerical simulation.

## 5 Results and discussion

### 5.1 Bending angle

Fig. 4 shows the experimental and numerical results of the bending angle vs. scanning speed. It is obvious that with increasing scanning speed, the heat input by laser decreases so that the bending angle reduces. It can be seen from Fig. 4 that the simulation results agree with the experimental measurements. More parametric studies and validations will be shown in subsequent discussion.

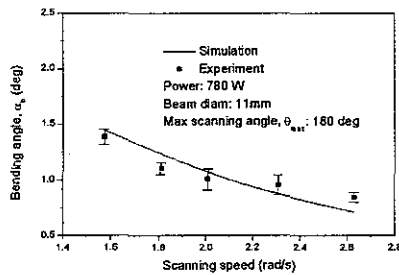


Fig. 4 Comparison of numerical, and experimental results (tube outer diameter: 12.7mm, wall thickness: 0.89mm)

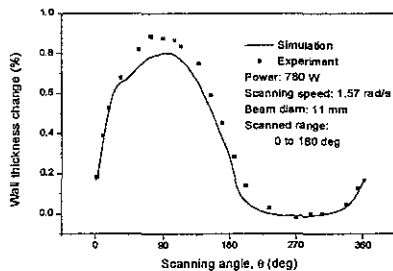


Fig. 7 Wall thickness variation at the scanning plane (tube outer diameter: 12.7mm, wall thickness: 0.89mm)

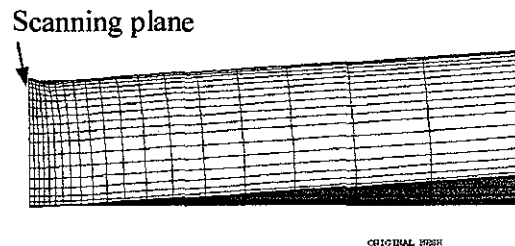


Fig. 6 Simulation of laser bent tube (magnification  $\times 5$ , half tube is shown due to symmetry, power: 780 W, scanning speed: 1.57 rad/s, beam diameter: 11mm,  $\theta_{max}$ : 180 degree, tube outer diameter: 12.7mm, wall thickness: 0.89mm)

### 5.2 Variation in the wall thickness

The simulated shape of a laser formed tube is shown in Fig. 6 and compared with the undeformed one. Only half of the tube was simulated due to the symmetry of the deformation about the scanning plane. It can be seen that the material in the intrados moves outward in the radial direction and shortened in the longitudinal direction as indicated by the distorted mesh. The experimental and simulated change in wall thickness is shown in Fig. 7. As expected, the maximum thickening of less than 1% occurs at the intrados, while there is no appreciable thinning at the extrados. This is one of the major advantages of the

laser bending process of tubes. To help understand the pattern of wall thickness variation, plastic strain in the axial direction at the outer and inner surfaces is plotted in Fig. 8(a), and that in the radial direction in Fig. 8(b). As seen, the amount of axial compressive strain caused by thermal expansion is approximately matched by the radial tensile strain as required by the rule of volume constancy<sup>6</sup>. Shown in Fig. 8(c) is the contour plot of the radial plastic strain in the scanning plane.

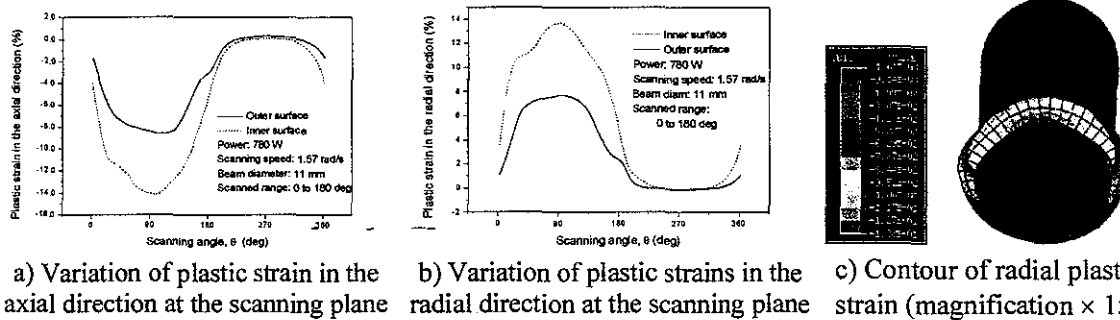


Fig. 8 Wall thickening and associated plastic strains (power: 780 W, scanning speed: 1.57 rad/s, beam diameter: 11mm, max scanning angle: 180 degree, tube outer diameter: 12.7mm, wall thickness: 0.89mm)

### 5.3 Inner surface of the scanned region

Fig. 9 presents the experimental and numerical results of the axial cross section of a laser-formed tube. It is interesting to note that the inner surface of the scanned region exhibits an outward bulge radially, which is counterintuitive, as the region was thickened during the bending process. This can be explained by the vertical component of the circumferential stress indicated in Fig. 2, which also explains why the axial plastic strain at the outer surface is smaller than that at the inner surface (Fig. 8(a)).

### 5.4 Ovalization of the cross section

Fig. 10 shows numerical and experimental results of ovalization of the bent tube vs. laser power used. The ovalization is defined as  $(D_{max} - D_{min})/D$ , where  $D_{max}$  and  $D_{min}$  are the maximum and minimum deformed diameters, respectively, and  $D$  is the undeformed tube diameter. As seen from Fig. 11, at the beginning and end of laser scanning (about  $1^\circ$  and  $180^\circ$ ), the outward displacement stated earlier is more intensive due to the stronger constraint from the surrounding material as compared to the middle region of the scanning (about  $90^\circ$ ). At about  $270^\circ$ , the middle of the unscanned region, the radial displacement is naturally zero. Therefore, the elongation in the horizontal direction is greater than that in the vertical direction and an oval cross section is formed. With increasing laser power, the situation just mentioned becomes more pronounced and ovalization increases, although it remains much smaller than that seen in mechanical bending of tubes. In mechanical bending of tubes, the magnitude of ovalization can reach 20% for some bending processes without a mandrel<sup>7</sup>.

### 5.5 Hardness

The hardness of the laser bent tube was measured and the variation of the hardness along the tube circumference is shown in Fig. 12. It can be seen that hardness increases in the laser-

scanned region and reaches a maximum value in the middle of the region (about 90°). One of the reasons for this is the strain hardening due to plastic deformation as shown in Figs. 8(a) and 8(b).

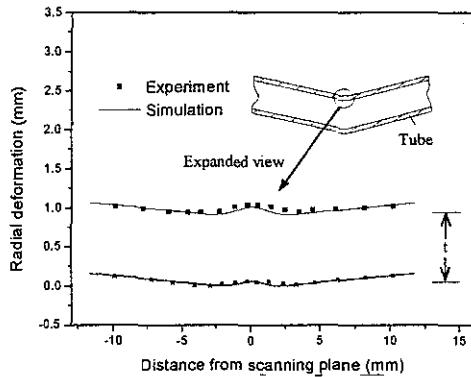


Fig. 9 Simulation and experimental measurements of the protruded intrados at the axial cross section ( $t$ : original wall thickness, power: 780 W, scanning speed: 1.57 rad/s, beam diameter: 11mm, maximum scanning angle,  $\theta_{max}$ : 180 degree, tube outer diameter: 12.7mm, wall thickness: 0.89mm)

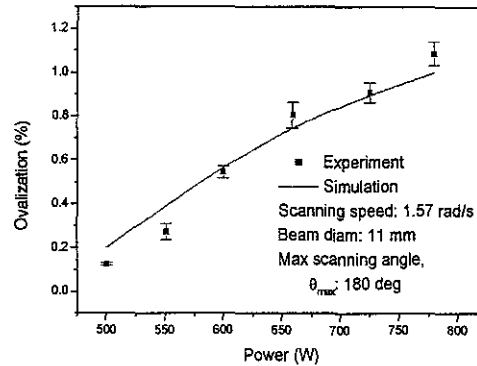


Fig. 10 Simulation and experimental results of ovalization of the cross section at the scanning plane (tube outer diameter: 12.7mm, wall thickness: 0.89mm)

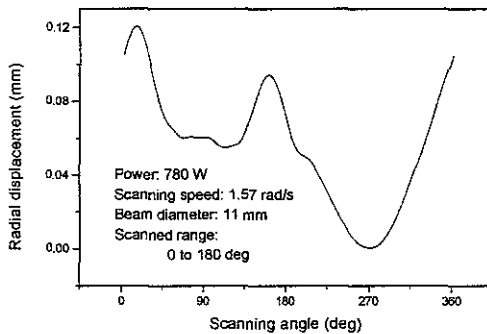


Fig. 11 Simulation results of the radial displacements of the outer surface of the scanning plane (tube outer diameter: 12.7mm, wall thickness: 0.89mm)

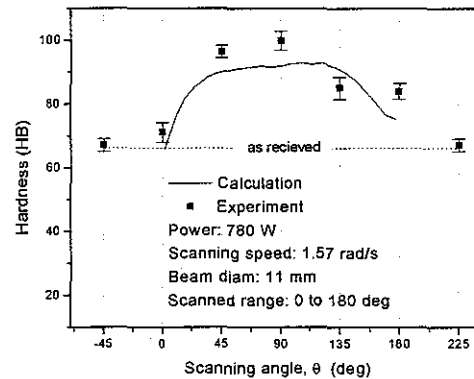


Fig. 12 Variation of hardness along the circumferential direction (tube outer diameter: 12.7mm, wall thickness: 0.89mm)

These figures show the variation of the plastic deformations has the same tendency as the hardness. The strain hardening increases the flow stress of the formed material, and there is an empirical relationship between flow stress and hardness for steel<sup>8</sup>. The calculation result is also shown in Fig. 12. It can be seen that the calculated values are slightly lower than the experimental ones. A possible reason for the discrepancy is that microstructure change may take place during the fast temperature rise and fall. This will be further discussed in the next section.

## 5.6 Microstructure

Fig. 13 shows SEM micrographs of the samples from the scanned region before and after laser bending. The microstructure of the unprocessed low carbon steel tube is a typical hypoeutectoid mixture of ferrite and pearlite (Fig. 13 (a)). Under the condition of natural air cooling, the microstructure of the bent tube at  $\theta=90$  degrees is shown in Fig. 13 (b). The micrograph

suggests that bainite has formed. With forced air cooling (35 kPa), at the same location, martensite has been partially observed (Fig. 13(c)). As seen, the laser-forming process may impart beneficial effects such as bainite structure or undesirable effects such as martensite structure on the formed parts depending on the process parameters used. The hardness increase shown in Fig. 12 could be also partially due to the microstructure changes just mentioned.

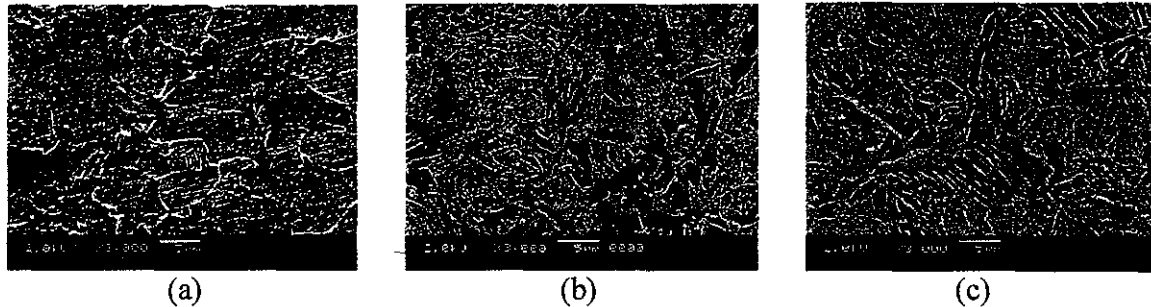


Fig. 13 Microstructure of the laser formed tube at  $\theta = 90^\circ$  (a) as received, (b) still air cooling, and (c) forced air cooling (power: 780 W, scanning speed: 1.57 rad/s, beam diameter: 11mm, maximum scanning angle,  $\theta_{max}$ : 180 degree, tube outer diameter: 12.7mm, wall thickness: 0.89mm).

### 5.7 Asymmetry

Fig. 8(c) shows the formed tube is asymmetry about the vertical axis. This is further shown in a top view in Fig. 14(a). It can be seen that the bent tube slightly tilts rightwards because the temperature at the end of scanning is higher than that at the beginning as shown in Fig. 14(b). Higher temperature produces more deformation in the axial direction. As a result, the centerline of the bent tube shifts rightward as shown in Fig. 14(a).

To overcome the asymmetry, one may employ different process parameters or scanning schemes. One of the options is to scan using a varying angular speed. Increasing the scanning speed near the end of the scanning can reduce the temperature there. Fig. 15(a) shows that the deformation becomes more symmetric. This is due to the more symmetric temperature along the circumferential direction effected by an empirically determined speed profile (Fig. 15(b)). Another approach examined in this work is to use a two-segment scanning scheme, that is, first scanning from 0 to 90 degrees, and then from 180 to 90 degrees (Fig. 16). The variation of the maximum temperature obtained from this scheme is also shown in Fig. 16. As seen, temperature is more symmetric about the vertical axis, and as a result, the deformed shape is more symmetric, similar to the case shown in Fig. 15(a).

### 5.8 Effect of the maximum scanning angle

So far, only bending results under  $\theta_{max} = 180^\circ$  have been presented. The effect of maximum scanning angle,  $\theta_{max}$  on the bending angle is shown in Fig. 17. Under the conditions examined, the bending angle increases with  $\theta_{max}$  to a maximum value, before it drops. As a tube is laser bent, the material in the scanned region is shortened and the material of the un-scanned region is bent by the moment caused by the shortening. With  $\theta_{max}$  increasing, the un-scanned region reduces. This makes the resistance against bending of this region lower so that the bending angle

risers. When  $\theta_{max}$  further increases, the tube tends to be scanned along its entire circumference and as a result, the bending efficiency drops.

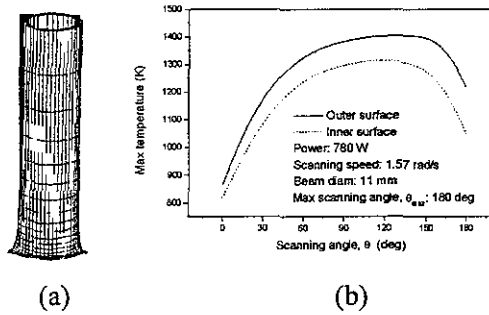


Fig. 14 (a) Asymmetry of deformation, i.e., tilting rightwards as seen from this topview (half tube shown due to symmetry about the scanning plane, magnification  $\times 20$ ), and (b) Variation of maximum temperature under the constant scanning speed (tube outer diameter: 12.7mm, wall thickness: 0.89mm)

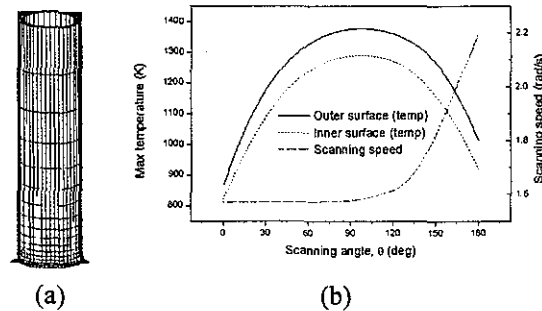


Fig. 15 (a) Improvement of symmetry by varying the scanning speed (half tube is shown, magnification  $\times 20$ ), (b) Variation of maximum temperature under the varying scanning speed (power: 780 W, beam diameter: 11 mm, max scanning angle,  $\theta_{max}$ : 180 deg, tube outer diameter: 12.7mm, wall thickness: 0.89mm)

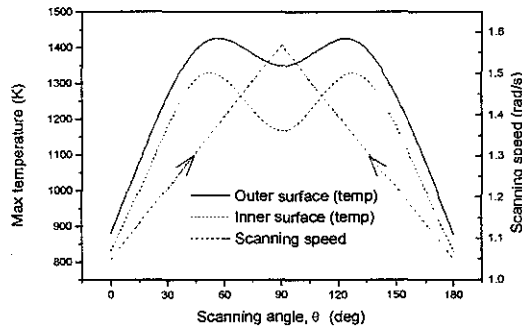


Fig. 16 Variation of maximum temperature under the two-segment scanning scheme ( $0^\circ$  to  $90^\circ$  and then  $180^\circ$  to  $90^\circ$ ) (power: 780 W, beam diameter: 11 mm, max scanning angle,  $\theta_{max}$ : 180 deg, tube outer diameter: 12.7mm, wall thickness: 0.89mm).

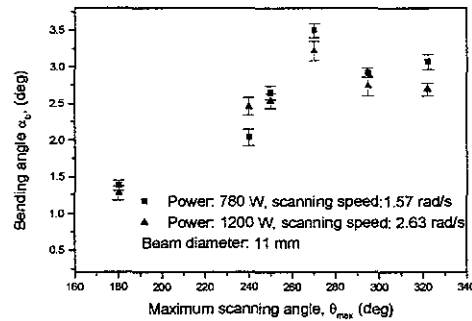


Fig. 17 Variation of the bending angle with the max scanning angle (tube outer diameter: 12.7mm, wall thickness: 0.89mm).

### 5.9 Beam diameter, tube size, and minimum bending radius

The influence of the laser beam diameter on the bending angle is presented in Fig. 18 for different ratios of the tube outer diameter,  $D$ , to the wall thickness,  $t$ . The bending angle decreases with increasing beam diameter because of the reduced laser intensity. The bending angle also decreases with increasing ratio  $D/t$ . As the ratio increases, the distance between the scanned and un-scanned regions increases but the shortening of the scanned region remains approximately unchanged. As a result, the bending angle decreases.

Fig. 19 shows the dependence of the average curvature radius on the laser beam diameter. As seen, the curvature radius increases with the beam diameter. This is because the dimension of the deformed area in the axial direction increases and thus the arc length of the curved region.

At the same time, the bending angle decreases due to reduced energy intensity (Fig. 18). Both result in rise of the curvature radius. It can also be seen from Fig. 19 that the curvature radius increases with the outer diameter/thickness ratio,  $D/t$ . With increasing ratio, the bending angle decreases while the arc length of the curved region remain more or less unchanged. As a result, the curvature radius increases.

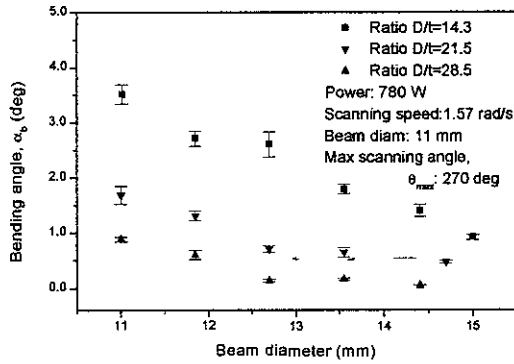


Fig. 18 Dependence of the bending angle on the beam diameter for different ratios of tube outer diameter,  $D$ , to wall thickness,  $t$  ( $t = 0.89$  mm)

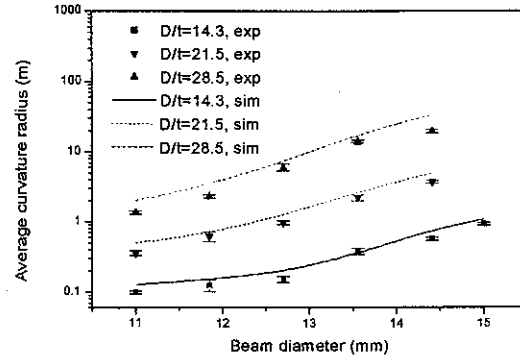


Fig. 19 Average curvature radius of the bent tube vs. beam diameter for different ratios of outer diameter vs. wall thickness (power: 780 W, scanning speed: 1.57 rad/s, maximum scanning angle: 270 degree, wall thickness: 0.89mm)

For mechanical bending, the minimum bending radius is mainly governed by the elongation of the material at the extrados and the tube outer diameter<sup>9</sup>. For laser bending of tubes, there is little elongation at the extrados and therefore the elongation is not a determining factor of the minimal bending radius. As seen from Fig. 19, the smaller the beam size, the smaller the average radius of curvature. But the upsetting mechanism of laser bending of tubes requires the beam diameter at least ten times of the tube thickness. At the same time, the smaller the outer diameter/thickness ratio is, the smaller the average radius of curvature. Therefore it is reasonable to conclude that the minimal bending radius in laser forming of tubes depends on laser beam size, tube thickness and outer diameter for most metallic materials. For extremely brittle materials that can not stand any elongation at the extrados, of course, the material properties will also play a role.

## 6 Conclusions

The mechanisms of laser bending of tubes are a combination of thickening of the laser-scanned region due to thermally induced axial compressive stress, and a slightly outward displacement of the region caused by a component of the thermally induced circumferential compressive stress. As a result, bending is primarily achieved through the thickening of the scanned region instead of the thinning of the unscanned region, and the scanned region assumes a slightly protruded shape. The absence of appreciable wall thinning is one of the major advantages of laser bent tubes. Cross-section ovalization of the laser-bent tubes is also much smaller than that observed in comparable mechanical bent tubes due to lack of bending die and appreciable tensile stress/strain in the extrados. The bending radius is governed by the laser beam diameter, not by tensile failure at the extrados. The curvature radii of the bent tube increase with the beam diameter and the ratio of the tube outer diameter to the wall thickness. Effects of the bending process on

microstructure change could be beneficial depending on process conditions. The bending efficiency increases with the maximum scanning angle up to a critical value. Asymmetry of the bending process can be reduced by varying the scanning speed or employing a two-segment scanning scheme.

### Acknowledgment

Support by NSF under Grant DMII-0000081 is gratefully acknowledged.

### References

- [1] Silve, S., Steen, W. M., and Podschies, B., 1998, "Laser forming tubes: a discussion of principles," Proceedings of ICALEO, Section E, 1998, pp. 151-160.
- [2] Frackiewicz, H., Trampczynski, W., and Przetakiewicz, W., 1992, "Shaping of tubes by laser beam," Proceedings of the 25<sup>th</sup> International Symposium on Automotive Technology and Automation, ISATA 25<sup>th</sup>, pp.373-380.
- [3] Kraus, J., 1997, "Basic process in laser bending of extrusion using the upsetting mechanism," Laser Assisted Net shape Engineering 2, Proceedings of the LANE'97, Meisenbach Bamberg, Germany, Vol.2, pp. 431-438.
- [4] Li, W. and Yao, Y. L., 1999, "Convex Laser forming with high certainty," Trans. North American Manufacturing Research Conference XXVIII, Lexington, KY, May, 2000, pp.33-38.
- [5] Li, W. and Yao, Y. L., 1999, "Effects of Strain Rate in Laser Forming," *Proc. 18th Int. Congress on Applications of Lasers and Electro-Optics (ICALEO '99): Conf. on Laser Materials Processing*, San Diego, Nov., 1999, Section F, pp. 107-116.
- [6] Lange, K., Pohlandt, K., Raghupathi, P.S., et al., 1985, "Handbook of metal forming," McGraw-Hill Book Company.
- [7] Pan, K. and Stelson K. A., 1995, "On the plastic deformation of a tube during bending," Transactions of the ASME, Journal of Engineering for Industry, Vol. 117, pp494-500.
- [8] Li, W. and Yao, Y. L., 1999c, "Laser forming with constant line energy," *The International Journal of Advanced Manufacturing Technology*, *accepted*.
- [9] Kervick, R. J. and Springborn, R. K., 1966, "Cold bending and forming tube and other section," ASTME, Michigan.

### Meet the Authors

Wenchuan Li is currently a Ph.D. candidate and Y. Lawrence Yao an Associate Professor in the Department of Mechanical Engineering at Columbia University, where Yao also directs the Manufacturing Engineering Program. Yao has a Ph.D. from Univ. of Wisconsin-Madison.